Impedance of a Single Intercalation Particle and of Non-Homogeneous, Multilayered Porous Composite Electrodes for Li-ion Batteries

ARTICLE *in* THE JOURNAL OF PHYSICAL CHEMISTRY B · JULY 2004

Impact Factor: 3.3 · DOI: 10.1021/jp0486402

2 AUTHORS:

Levi Mikhael
Bar Ilan University
193 PUBLICATIONS **8,739** CITATIONS
SEE PROFILE

Doron Aurbach
Bar Ilan University
537 PUBLICATIONS **21,873** CITATIONS
SEE PROFILE

Impedance of a Single Intercalation Particle and of Non-Homogeneous, Multilayered Porous Composite Electrodes for Li-ion Batteries

M. D Levi* and D. Aurbach

Department of Chemistry,Bar-Ilan University, Ramat-Gan 52900, Israel

Received: March 28, 2004; In Final Form: May 3, 2004

Some peculiar features of impedance spectra of a variety of porous, composite Li insertion electrodes, such as the formation of arcs and semicircles in Nyquist plots related to low frequencies are discussed. A new model that takes into account the possible nonhomogeneous (layered) distribution of the electrode's active mass on the current collector was developed. Each porous layer in the composite electrode consists of spherical particles, which insert lithium reversibly. We show that the appearance of a low-frequency semicircle (Nyquist plots) with a high capacitance value, rather than an arc or sloping lines, could be understood by adopting a nonhomogeneous, layered distribution model of the electrode's active mass, and finite values of the conductivity of the solid particle and the solution in the electrode's pores. Evidence was presented (supported by model calculations) that the low frequency semicircles observed in the Nyquist plots of these composite electrodes originate from a parallel combination of a low-frequency response of the intercalation capacity of the thinner parts and an active, highly resistive component of the impedance of the thicker parts of the electrode. A detailed comparison between the finite-space diffusion elements for spherical and linear (slab) particles is also presented.

Introduction

There have been recent developments related to the fabrication of single intercalation particle electrodes and their electroanalytical characterizations using a vast arsenal of precise electroanalytical tools, of which electrochemical impedance spectroscopy is the most important.[1−8] It is very interesting and important to compare these electrochemical responses with the many responses obtained in our research group from practical porous composite electrodes for rechargeable Li-ion batteries,[9−16] (see also a review paper[17]). Our early, highly resolved EIS and slow-scan rate cyclic voltammetric characterizations (SSCV) data for thin graphite electrodes during Li-ion intercalation[9,10,17] were interpreted within the framework of a simple model: the porous electrode was assumed to be constructed by an array of individual particles that intercalate independently with Li-ions from the surrounding solution, and in parallel. Thus, the thin composite electrodes were assumed to be uniformly accessible throughout their depth. If the porous layer thickness is reasonably small, and the charging rate is slow enough, this simple model of parallel working individual particles of the composite electrodes seems to be useful for the interpretation of the electroanalytical responses obtained from these electrodes. Later, we developed a two-parallel diffusion paths model[18] that described simultaneously the responses obtained by parallel EIS and PITT (potentiostatic intermittent titration technique) characterizations, and could be applied to the responses of the porous electrode under conditions of infinitely high electronic particle bulk and ionic pore solution conductivities, σ and κ, respectively.

Recently, an important theoretical model of Meyers et al.[19] for the impedance response of a porous intercalation electrode has been published, and which treats specifically the case of small values of σ and κ. Qualitatively, the effect of low σ and κ can be understood in terms of Ohmic potential drops in the pores filled with the solution and in the solid phase, which leads to a typical, low-frequency impedance response that reflects distribution elements.[19] This particular type of dispersion of the low-frequency capacitance of porous, composite electrodes is due to coupling of interfacial and bulk quantities, as was suggested by Pajkossy[20] in his treatment of the impedance of rough capacitive electrodes.

In the present paper, we address the problem of the formation of low-frequency semicircles in the impedance spectra presented as Nyquist plots for most of the practical, composite intercalation electrodes (which typically reflect high capacitance calculated from their Z''_{max}). Whereas, none of these features was observed with the corresponding single-particle electrodes (see a series of publications by Uchida et al.[1−7]). We show that these specific features of the low-frequency impedance of composite electrodes could be elucidated by adopting a nonhomogeneous, layered distribution of the electrode's active mass on the current collector. Each sublayer can be described within the framework of the Meyers et al model.[19]

In this paper we first consider the relation between the previously published two-parallel-diffusion-paths model[18] and the present model, taking into account the effects of slow intercalation kinetics and double-layer charging. We will then compare impedance spectra simulated with the use of linear and spherical finite-space diffusion models. The last sub sections deal with a comparison of our model and that published by Meyers et al.[19] with the emphasis on the origin of the arcs and the semicircles (Nyquist plots) with a high characteristic capacitance, which usually appear in the low-frequency domain of the impedance spectra of porous, composite electrodes.

2. Results and Discussion

2.1. Relation Between a Previous Two-Parallel-Diffusion-Path Model and the Present Model. Figure 1a presents a general equivalent circuit analogue of the process of ion insertion

* To whom correspondence should be addressed.

10.1021/jp0486402 CCC: $27.50
Published on Web 07/03/2004

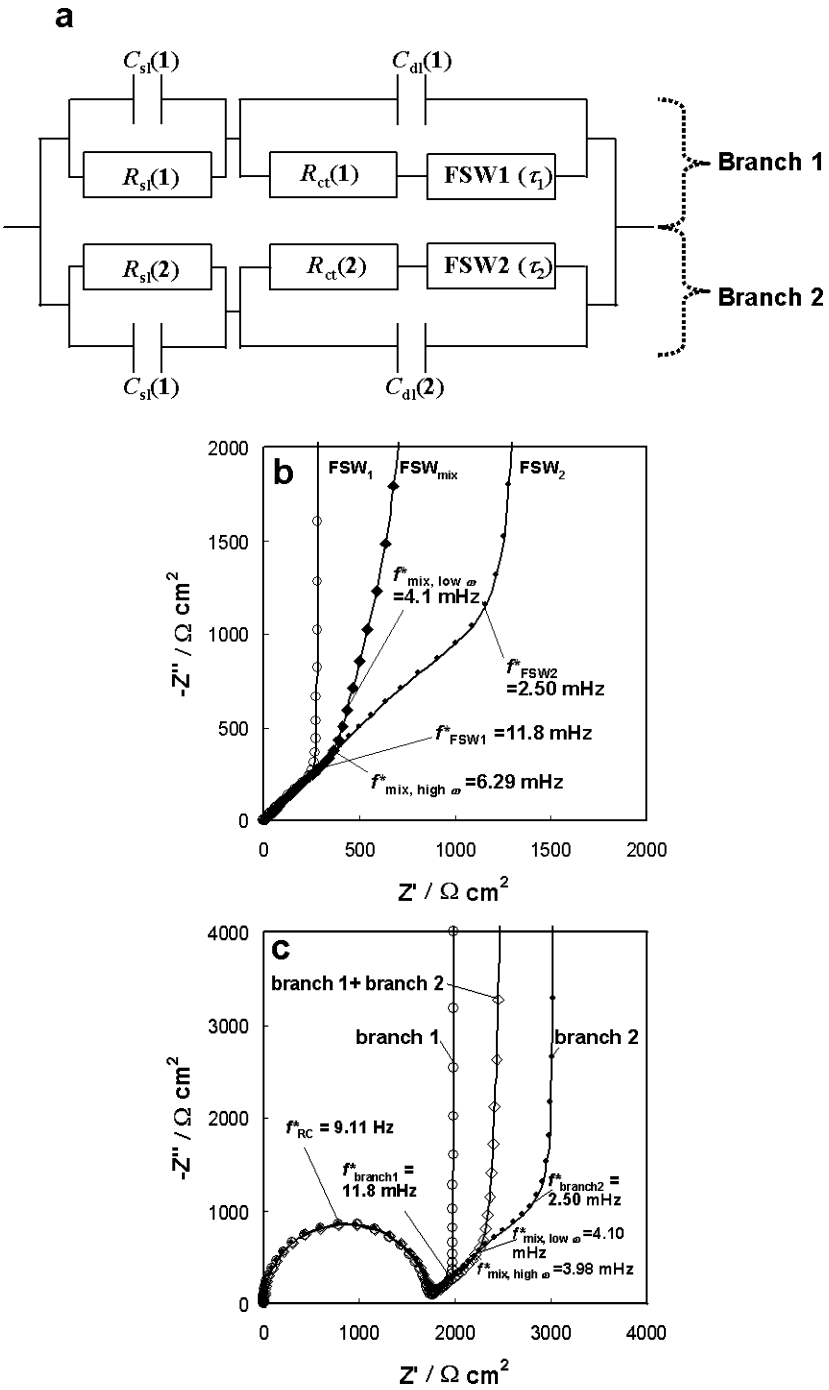

Figure 1. (a) Equivalent circuit analogue for a two-parallel diffusion paths model accounting for the ion migration through the surface layer covering each particle (high-frequency $R_{sl}||C_{sl}$ semicircle, with R_{sl} and C_{sl} standing for the resistance of the migration and capacity of the layer, respectively), double-layer charging and slow interfacial ion-transfer transfer (middle-frequency $R_{ct}||C_{dl}$ semicircle, with R_{ct} and C_{dl} designating the related charge-transfer resistance and a double-layer capacitance) and a finite-diffusion Warburg element, FSW. Indices 1 and 2 refer to path (branch) 1 and 2, respectively; (b) and (c) show simulated impedance spectra with the use of the above circuit analogue and eqs 4 and 5 for the two cases: without (b) and with (c) double-layer charging and slow charge transfer kinetics, respectively (in this particular simulation the particles are supposed to be free of surface films, thus $R_{sl} = 0$ *and* $C_{sl} = 0$). Parameters used in the simulation were as follows. In branch 1: FSW1 $- \tau_1/C_{dif} = 850\ \Omega cm^2$; $\tau_1 = 85$ s; $C_{dl} = 10\ \mu Fcm^{-2}$; $R_{ct,1} = 1700\ \Omega cm^2$. In branch 2 FSW1 $- \tau_2/C_{dif} = 4000\ \Omega cm^2$; $\tau_2 = 400$ s; $C_{dl} = 10\ \mu Fcm^{-2}$; $R_{ct,2} = 1700\ \Omega cm^2$. C_{dif} in both cases was 0.1 F. The values of the impedance were referred to 1 cm^2 of particle surfaces. Transition frequencies, f^*, of high-frequency semicircles and characteristic frequencies of the FSW elements are indicated.

into a composite electrode comprising two types of particles, having, for example, a different size, whereas all the other parameters (specific double layer capacitance, charge-transfer resistance, resistance and capacitance of the surface layers covering these particles, etc.) remain virtually the same. The major difference in the kinetics of ion intercalation into these particles is then simply reduced to the difference in the rate of finite-space diffusion inside these particles owing to the difference in the diffusion lengths. In this case, one can neglect all the contributions to the total impedance indicated in Figure 1a, except for two finite-space Warburg (FSW) elements presented in the parallel branches in this figure (1 and 2). We have recently reported[18] in detail the properties of this model, considering the case of linear diffusion, that is, the intercalation particles were assumed to be slab shaped, whose wide dimension was identified with the characteristic diffusion length. For linear,

finite space diffusion, the relevant Warburg-type element (i.e. the FSW) can be presented in the following, simple form:[21−31]

$$Z_{\mathrm{FSW},\,i} = \frac{\tau_i}{C_{\mathrm{dif},\,i}} \frac{\coth(\sqrt{j\omega\tau_i})}{\sqrt{j\omega\tau_i}} \tag{1}$$

where Z_{FSW} is the related impedance, that is, the transfer function between the alternating current and the voltage at a small amplitude of perturbation, and $\omega = 2\pi f$ is the angular frequency with f representing the alternating voltage frequency; τ and C_{dif} are the characteristic diffusion time constant and the low-frequency differential intercalation capacitance, respectively. Sub index i may be 1 or 2, designating one or the other individual particle path (branch) of the circuit analogue in Figure 1a.

A parallel combination of two FSW elements with different values of τ_i has a remarkable property, which may serve as an indicator for the branching of the intercalation paths.[18,32] An analysis of this combination shows that there should be two different diffusion time constants typical of the high and low-frequency domains (i.e., $\tau_{\mathrm{mix,high}\ \omega}$ and $\tau_{\mathrm{mix,low}\ \omega}$), in contrast to the same value of τ for a single path diffusion (i.e. for a homogeneous intercalation process). The term τ_{mix} means that the electrodes under study contain a mixture of particles or diffusion paths of different (mix) diffusion time constants. The related expressions for the values that can be deduced from the impedance spectra τ are as follows:[18,32]

$$\frac{1}{\sqrt{\tau_{\mathrm{mix}}^{\mathrm{high}\omega}}} = \frac{\theta_1}{\sqrt{\tau_1}} + \frac{1-\theta_1}{\sqrt{\tau_2}} \tag{2}$$

and

$$\tau_{mix}^{\mathrm{low}\omega} = \theta_1\,\tau_1 + (1-\theta_1)\,\tau_2 \tag{3}$$

where θ_1 is a fraction to which path 1 participates in the parallel intercalation process (a fraction of the total capacitance).

Equations 2 and 3 are derived from the expression of the *coth*-function in the limit of the very high and low frequencies, respectively. At high frequencies, FSW reduces to a classical semi-infinite Warburg element,[29] and thus a parallel combination of two FSWs results in averaging the related Warburg constants, which, in turn, are inversely proportional to the square root of the chemical diffusion coefficient, $D_s^{1/2}$, and hence proportional to $\tau^{1/2}$. The weighted sum of reciprocals of $\tau^{1/2}$ thus relate to a parallel combination of the Warburg constants. In contrast, in the limit of low frequencies, Z_{FSW} is mainly controlled by the differential intercalation capacitance C_{dif}, whose parallel combination in the two paths model results in averaging C_{dif} (with fractions $\theta_{1,2}$) and thus τ_i, in accordance with eq 3, since the finite space-diffusion model predicts proportionality between C_{dif} and τ_i.[18,32] Rubinstein et al.[32] derived eqs 2 and 3, considering only these two limiting cases, whereas eq 1 can be useful for the characterization of the intermediate frequency domains.[18]

Figure 1b illustrates the effect of the difference in the diffusion time constants on the shape of the Nyquist plots calculated for two individual branches (i.e. particles with different values of τ_i), and for their parallel combination at an equal fraction of their participation in the intercalation process ($\theta_1 = \theta_2 = 0.5$). Two different values of τ_i for the mixture result in a specific distortion of the shape of the Nyquist plot, which can be recognized even visually in Figure 1b (compare with the plots for individual FSWs).

2.2. Effect of Slow Interfacial Kinetics and Double Layer Charging. If a double layer charging (i.e., the differential capacitance $C_{\mathrm{dl},i}$ in Figure 1a) and a slow ion transfer (characterized by the resistance $R_{\mathrm{ct},i}$ in Figure 1a) affect the faradaic impedance of the active mass, (i.e., host particles that insert lithium), the admittance response of the mixture of the particles on the electrode should appear as an average between the admittances of the various particles (represented by individual branches in the analogue circuit shown in Figure 1a). The impedance for each branch can be presented in the following form:

$$Z_{\mathrm{branch,i}} = \frac{R_{\mathrm{ct},i} + Z_{\mathrm{FSW},i}}{1 + j\omega\, C_{\mathrm{dl},i}(R_{\mathrm{ct},i} + Z_{\mathrm{FSW},i})} + \frac{R_{\mathrm{sl},i}}{1 + j\omega\, R_{\mathrm{sl},\,i} C_{\mathrm{sl},\,i}} \tag{4}$$

The last term in eq 4 relates to possible surface film contribution to the impedance (see section 2.5). The admittance related to an electrode comprising a mixture of the particles, can be conveniently presented in the framework of a model containing parallel branches as follows:

$$\frac{1}{Z_{\mathrm{mix}}} = \frac{\theta_1}{Z_{\mathrm{branch},1}} + \frac{(1-\theta_1)}{Z_{\mathrm{branch},2}} \tag{5}$$

Figure 1c shows Nyquist plots for individual branches, and the mixture ($\theta_1 = 0.5$) calculated by the use of eqs 4 and 5. The parameters of the individual FSW elements in this simulation remain the same as those in Figure 1b. However, a relatively large interfacial kinetics contribution ($R_{\mathrm{ct},1} = 1700\ \Omega\mathrm{cm}^2$, $C_{\mathrm{dl}} = 10\ \mu\mathrm{Fcm}^{-2}$) was taken into account. When comparing impedance spectra for a mixture of particles in Figs. 1b and c, one can easily see that the resistive component of the kinetics contribution flattens the curve in the latter figure. The values of the characteristic frequencies calculated from the low and the high frequency domains appear to be virtually the same, 4.10 and 3.98 mHz, respectively. This extreme example (large kinetics contribution) shows that the mixture of particles behaves in a quasihomogeneous manner. To visualize the effect of nonhomogeneity (i.e., returning to the results of Figure 1b), one should subtract the kinetics contributions from the total impedance, that is, to perform a complete analysis of the impedance structure.

2.3. Finite-Space Diffusion for a Spherical Particle in Comparison with the FSW for a Linear Diffusion. There are only a few practical intercalation electrodes that meet the conditions of a linear (slab) finite-space diffusion model. Most of the intercalation particles have a rounded shape, and thus the simplest approximation should be a spherical particle. These particles may form composite porous electrodes, as shown schematically in Figure 2. Meyers et al.[19] derived an expression for the impedance of such an electrode composed of particles of different sizes and different particle size distribution. (For simplicity, we will consider two-particle size distribution only, i.e., two particles with $R_{\mathrm{s},1}$ and $R_{\mathrm{s},2}$ radii). As will be seen from further analysis of the expression of the impedance of a porous electrode at constant thickness, L, it is impossible to reproduce a well-developed low-frequency semicircle of the impedance spectra reported, for example, for a variety of composite graphite electrodes.[11,33] To solve this problem, we assume that the composite electrode coating is not geometrically homogeneous, and instead of a single value of the coating's thickness L, there may be a distribution of L. To understand the essential properties of this model, we consider herein a simplified system, which is an electrode comprising two layers having thicknesses of L_1

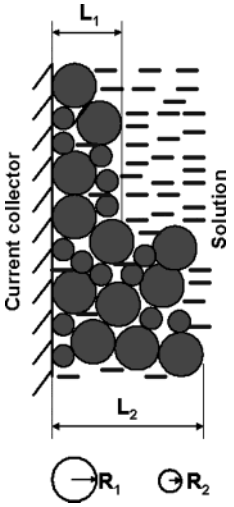

Figure 2. Schematic view of a general model of two spherical particle size distributions (radius $R_{s,1}$ and $R_{s,2}$) occurring in two layers of different thicknesses L_1 and L_2 (inhomogeneous layered coating). The homogeneous case is considered first ($L_1 = L_2$).

and L_2, contributing to the total charging by θ_L and $(1 - \theta_L)$; θ_L varies from 0 to 1. However, prior to the derivation of an expression for the impedance for such a model porous electrode, we need to specify the impedance of a single individual spherical particle.

A solution to the diffusion equation for spherical particles has been reported by Armstrong,[34] Jacobsen and West,[35] and generalized recently by Meyers et al.[19] For the purpose of comparing their results with a linear FSW expression (eq 4), impedance of a single spherical particle can be conveniently presented in the following form:[19]

$$Z_{\text{faradaic},\,i} = R_{\text{ct},i} + \frac{R_{\text{part},i}}{Y_{\text{s},i}} = R_{\text{ct},i} + R_{\text{part},\,i}\frac{\tanh(\sqrt{j\,\omega\,\tau_i})}{(\sqrt{j\,\omega\,\tau_i} - \tanh(\sqrt{j\,\omega\,\tau_i}))} \quad (6)$$

A comparison of eq 6 with eq 4 shows that $(1/Y_{s,i})$, which is equal to the fraction of the second right-hand term of eq 6, is a spherical analogue of the characteristic function of frequency in the expression for a linear FSW element, i.e., $\coth(\sqrt{j\omega\tau_i})$. The amplitude of the finite-space spherical diffusion element, $R_{\text{part},i}$, is determined similarly:[19]

$$R_{\text{part},i} = \frac{R^2_{\text{s},\,i}}{3D_{\text{s}}C_{\text{part},\,i}} = \frac{\tau_{\,i}}{3C_{\text{part},\,i}} \quad (7)$$

with $C_{\text{part},i}$ standing for a limiting, low-frequency capacitance $C_{\text{part},i}$ for a spherical particle.

A closer inspection of the impedance behavior of a spherical particle, especially at moderately high frequencies, is required, since this particular frequency domain was characteristic of the deviation of Nyquist plots related to a mixed particles electrode from the classical, linear FSW behavior, as discussed above. Figure 3a presents a direct comparison of the diffusion for both particle's geometries. Diffusion time constant, differential intercalation capacitances, double layer capacitances, and charge-transfer resistance were chosen to be the same in both calculations (see the caption to Figure 3). The characteristic linear diffusion length l, and the radius of the spherical particles, R_s, were the same (2 μm). The volume of the spherical particle,

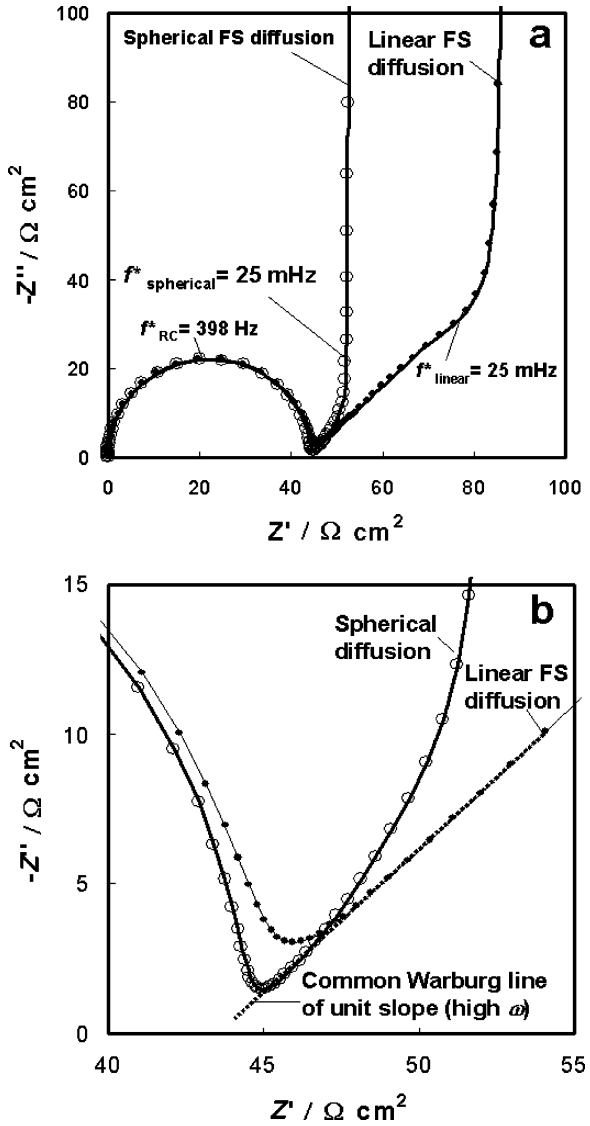

Figure 3. (a) Comparison of Nyquist plots calculated with the use of the circuit analogue (shown in Figure 1) for linear and spherical diffusion models. Diffusion time constant, differential intercalation capacitance, double layer capacitance, and charge-transfer resistance were chosen the same in both calculations (τ = 40 s, $C_{\text{dif}} = C_{\text{part}}$ = 0.317 Fcm^{-2}, C_{dl} = 10 μFcm^{-2}, R_{ct} = 44.06 Ωcm^2). The resistance of the FSW (see eq 1), τ/C_{dif} = 126.2 Ωcm^2). Simulation of the impedance curves for spherical diffusion was performed according to eq 6 for R_{part} = 42 Ωcm^2. The characteristic linear diffusion length, l, and the radius of a spherical particle, R_s, were the same (2 μm). The chemical diffusion coefficient ($D_s = 1 \times 10^{-9}$ cm^{2}s^{-1}) was always the same. (b) The same impedance spectra with a detailed view of the mixed, kinetic/diffusion domain. Note a common Warburg line in the limit of high frequency of the unit slope. The characteristic frequencies are indicated.

3.35×10^{-11} cm^3, was practically the same as that for the equivalent linear slab ($2lx2lxl$), 3.20×10^{-11} cm^3. However, the total surface of the slab was about 25% higher than that of the equivalent sphere, 6.4×10^{-7} and 5.07×10^{-7} cm^2, respectively. To avoid the difficult problem in distinguishing the difference between double-layer charging and surface films formation on the total surface of the slab and the charge-transfer in the direction of the diffusion (e.g., through the cross-sectional area), we arbitrarily assigned the same specific values of $R_{\text{ct},i}$ and $C_{\text{dl},i}$ for the spherical particle and the slab, neglecting the difference in their relevant surface areas. Also the same chemical diffusion coefficient ($D_s = 1 \times 10^{-9}$ cm^{2}s^{-1}), the diffusion time constants (τ_i = 40 s), and the low-frequency differential

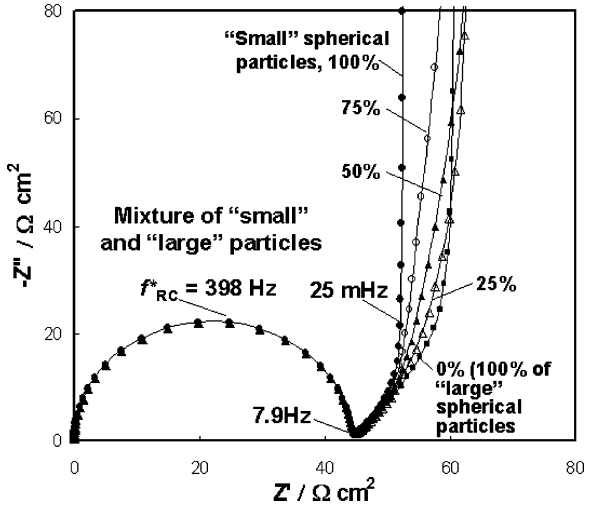

Figure 4. Impedance spectra for a mixture composed of "small particles" with a radius of $R_{s,1} = 2\ \mu$m, and the parameters indicated in the caption to Figure 3, and "large particles" with $R_{s,2} = 4\ \mu$m, $R_{part,2} = 84\ \Omega cm^2$; $\tau_2 = 160$ s; $C_{dl} = 10\ \mu F cm^{-2}$; $R_{ct,2} = 44.06\ \Omega cm^2$ ($D_s = 1 \times 10^{-9}$ cm^{2}s^{-1} and $C_{part,2} = 1.9$ F). Calculated with the use of eqs 5−7. The proportion between the two kinds of particles (percentage of small particles in the mixture) is indicated.

intercalation capacitances ($C_{dif} = C_{part} = 0.317\ F cm^{-2}$) were used. In the low-frequency domain, the impedance of a single particle electrode has the same limiting, capacitive behavior for both particles' geometries. However, qualitatively, the limiting, low-frequency resistance, R_L, is considerably less for the spherical diffusion case compared to the linear one, as is seen in Figure 3a.

An analysis of the limiting behaviors of eqs 4 and 6 in the low-frequency domain shows that $R_L = (1/5)R_{part}$ for spherical diffusion,[19] whereas for linear diffusion $R_L = (\tau/3C_{dif})$.[36] The characteristic frequency determining the transition from a semi-infinite diffusion at high frequencies to the capacitive behavior at low frequencies was the same for both cases (25 mHz), as marked on the curves of Figure 3a. It is seen that the capacitive behavior of the finite-space element for a spherical diffusion actually starts at much higher frequencies than those of the linear diffusion. Therefore, the length of the high frequency, semi-infinite Warburg behavior for the former diffusion is much shorter than that for the latter one, as is clearly seen from the mixed kinetic/diffusion domain of the spectra shown in Figure 3b. This is due to the fact that curvature of the particle affects the penetration depth at these low frequencies, although these frequencies are not so low so that the penetration depth reaches the particle's center[19]. Such an effect is obviously absent for the linear diffusion, for which the cross-sectional surface area is flat. A more capacitive character of the finite-space impedance of a spherical particle at intermediate frequencies, and a lower real component of its impedance compared to the related quantities for the linear diffusion, results in a better separation between the charge-transfer semicircle and the Warburg region, as can be seen in Figure 3b.

Using eq 6 for a single spherical particle impedance, we can now simulate the impedance spectra for a mixture of particles with radii $R_{s,1}$ and $R_{s,2}$, using eq 5 for this and varying the fraction of the first particle, θ_1, from 0 to 1. The results are presented in Figure 4. From an inspection of the curves in Figure 4 it can be concluded that the effect of mixing two particles is clearly seen on the related Nyquist plots in the form of a sloping, low-frequency capacitive line, in contrast to almost vertical lines for the single particles. The slope changes gradually with the value of θ_1 (see Figure 4); an early deviation from the limiting semi-infinite Warburg behavior towards capacitive behavior is typical of the mixtures as well as of the individual particles.

In the present study, we did not indicate the way in which particles of the mixture are arranged or how the space between the particles is filled with an electrolyte solution (instead, as was proposed by Meyers et al.,[19] two effective parameters of the porous structure can be used, namely, the porosity and the ratio of the total surface area to its volume, a, see later). The only requirement was that each particle contributes to the total intercalation process individually. When studying the low-frequency responses of porous graphite electrodes (mainly by slow scan rate cyclic voltammetry)[9,17] we proved that a porous electrode under *these conditions* may be in fact modeled as an array of individually operating particles. It is clear that this model could be extended to higher frequency domains, provided that both electronic and ionic conductivities of the individual solid particles (σ) and the ionic conductivity of the solution in the porous space between the particles (κ) would be infinitely high. If this is the case, there is a relationship between the impedance characteristics of a single particle (or an array of single particles) and those of a porous composite electrode that comprise such particles. The impedance of the porous electrode will be lower than that of single particles by a factor similar to the ratio between the high surface area of the porous electrode and that of the single particle (taking into account the true surface area of the porous electrode). Finite values of the above conductivities (which is certainly the real case) will result in a distributed nature of the porous electrode impedance, as was demonstrated by de Levie[37] for the distributed double-layer capacitances and pore solution resistances (see also the related discussion by Pajkossy[20]), and recently by Meyers et al.[19] for a porous electrode composed of intercalation particles.

2.4. Distributed Impedance of a Porous Electrode with Finite Values of σ and κ. To study the effect of σ and κ on the impedance of a mixed particle porous electrode, we used the approach of Meyers et al.[19] The impedance of a porous electrode, Z_{porous}, can be related to the impedance of a mixed particle electrode as follows:[19]

$$Z_{porous} = \frac{L}{\kappa + \sigma}\left[1 + \frac{2 + \left(\frac{\sigma}{\kappa} + \frac{\kappa}{\sigma}\right)\cosh \nu}{\nu \sinh \nu}\right] \qquad (8)$$

with a complex parameter ν of the form:

$$\nu = L\left(\frac{\kappa + \sigma}{\kappa\sigma}\right)^{1/2}\left(\frac{a}{Z_{mix}}\right)^{1/2} \qquad (9)$$

where κ and σ were earlier defined as the specific conductivities of the electrolyte solution and the solid particles, respectively, L is the porous electrode thickness, a denotes the ratio of the total surface area to its volume, and Z_{mix} is obtained from eq 5. In the specific case of $\theta_1 = 0$ or 1, the impedance will relate to a porous electrode composed of identical spherical particles. We first checked these equations to obtain an impedance spectrum of a porous electrode composed of identical spherical particles of an $R_s = 2\ \mu$m radius, with all the other parameters coinciding with those used in Meyers'et al. work.[19] In particular, κ and σ were equal to 55 μScm^{-1} and 1.0 Scm^{-1} (both values of 1000 Scm^{-1} were considered as infinitely high conductivity).

The results are shown in Figure 5, and they are identical to those obtained by Meyers et al.[19] A drastic change in the shape of the impedance for a porous electrode becomes evident when comparing it with the impedance plot for a single-particle

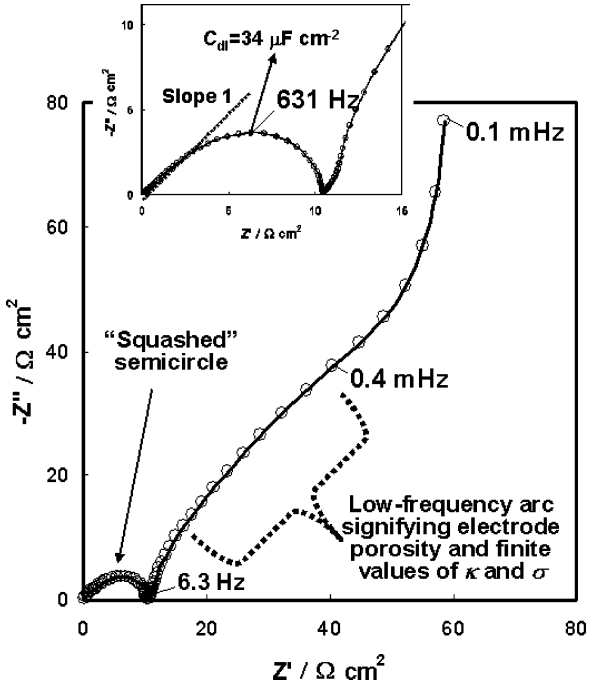

Figure 5. Simulated impedance spectra of a porous electrode composed only of "small" particles. Parameters of the impedance of an individual particle are indicated in the caption to Figure 3a. The parameters of the porous structure were as follows: $L_1 = 100$ μm, $a = 7500$ cm^{-1}, $\kappa = 55$ μS cm^{-1}, and $\sigma = 1.0$ S cm^{-1} (see eqs 8 and 9). Characteristic RC-frequency and an effective value of C_{dl} are indicated. Note the appearance of a low-frequency arc as a consequence of the porous electrode structure and finitely high values of κ and σ.

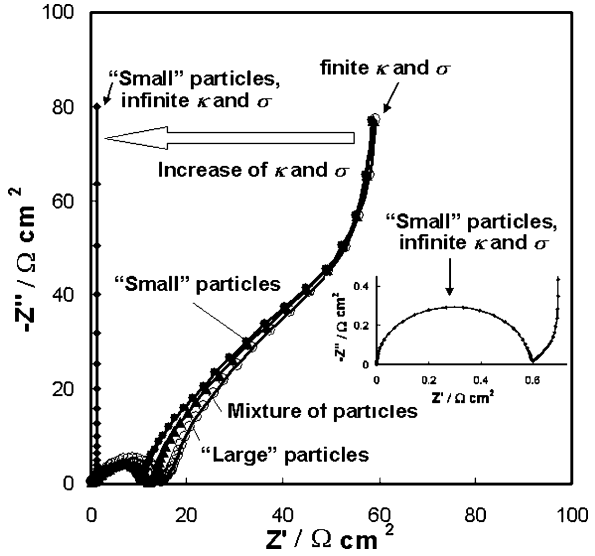

Figure 6. Comparison of impedance spectra for three different porous electrodes composed of (i) small particles only, (ii) large particles only, (iii) a mixture (1:1) of small and large particles. Parameters for the small particles' porous electrode are indicated in the caption to Figure 5. Parameters for individual large particles are indicated in the caption to Figure 4a. Parameters of the porous electrode structure as in Figure 5, except for a reduced value of $a = 3750$ cm^{-1} because of the lower total surface area of large particles compared to small ones, placed in a layer of the same thickness. The admittance of a porous electrode composed of a mixture of small and large particles (thickness as for the other two electrodes) was averaged according to eq 5. In all three calculations, finite values of $\kappa = 55$ μS cm^{-1} and $\sigma = 1.0$ S cm^{-1} were used. The left vertical line relates to the impedance spectrum for a porous electrode composed of small particles, which, in contrast to the family of three curves in the same figure, was calculated with $\kappa = 1 \times 10^3$S cm^{-1}, $\sigma = 1 \times 10^3$ S cm^{-1} (practically, infinitely high κ and σ). The inset shows the high-frequency domain of the spectrum for this electrode (note the absence of low-frequency arc).

electrode (compare with the left curve in Figure 3a). A squashed semicircle with an approximate unit slope appears in the Nyquist plot for the porous electrode in the limit of very high frequencies, which is due to the distributed character of the impedance at finite κ and σ, rather than to the semi-infinite nature of diffusion in this system.[19]

It is instructive to compare the values of the double-layer capacitance obtained from the high-frequency semicircle (HFS) at the characteristic frequency of 631 Hz. Note that C_{dl} for a single particle was taken to be 10 μF cm^{-2}. The impedance spectra in Figure 5 refer to 1 cm^2 of the surface area of the current collector. Thus, ignoring the real porous structure of the electrode, we can obtain from the HFS the value $C_{dl} = 34$ μF cm^{-2} (see inset in Figure 5), which is more than three times higher than that for the single particle. However, the electrode is actually porous, and if all the particles would contribute equally to the intercalation process, the total impedance in this frequency range should be much smaller, as shown in Figure 6 and in the inset of this figure for the same single particle porous electrode, but with infinitely high σ and κ. As has been already mentioned, impedance spectra for a single particle and the porous electrode composed of these particles have exactly the same structure and can be easily scaled, using the true surface area of the porous electrode: one square centimeter of the porous layer (100 μm thick) composed of spherical particles (radius 2 μm) was estimated to be 78 cm^2. This value can be easily obtained noting that the volume and the surface area of the individual particle are 3.35×10^{-11} cm^3 and 5.02×10^{-7} cm^2, respectively. In each layer, the particles occupy sites on a square lattice (the coordination number is 4) such that one complete layer contains 6.25×10^6 particles (per unit surface of the current collector). We assume that particles in the upper layers are located exactly above the particles in the first layer (thus the lattice is cubic). In this case, a 100-μm thick porous electrode (current collector of 1 cm^2) will contain 1.56×10^8 particles with the total surface area of 78 cm^2. Normalizing the impedance of the single particle by the surface area of 78 cm^2, we evaluate the diameter of the semicircle for the 100-μm porous layer as 0.56 Ω cm^{-2}, in good correspondence with 0.58 Ω cm^{-2} obtained with the use of the porous electrodes model (eqs 8 and 9) at infinitely high σ and κ (see inset in Figure 6). It is therefore not surprising that from the HFS in the inset in Figure 6 for the porous electrode (at infinitely high σ and κ), we recover the same value of $C_{dl} = 10$ μF cm^{-2} as for the single particle impedance.

In contrast, taking into account the total surface area of the 100-μm thick porous electrode, the double-layer capacitance for finite high σ and κ should be recalculated: $C_{dl} = 0.43$ μF cm^{-2}, which signifies that at high frequencies not all of the particles contribute to the impedance response, and thus the electrode's impedance becomes distributed.

The distributed character of the impedance of a porous electrode acquires pronounced typical features in the middle-frequency domain, which deviate completely from a semi-infinite Warburg-type behavior, as is seen from the characteristic arc shown in Figure 5. Obviously, any attempt to determine D_s from this region becomes meaningless without knowing exactly the porous structure of the electrode. With a further decrease in frequency, the impedance transforms into a vertical capacitive line. Very slow charging and discharging of some host particles results in a higher active mass utilization of the porous electrode so that from the value of $-Z''$ at the lowest "measured"

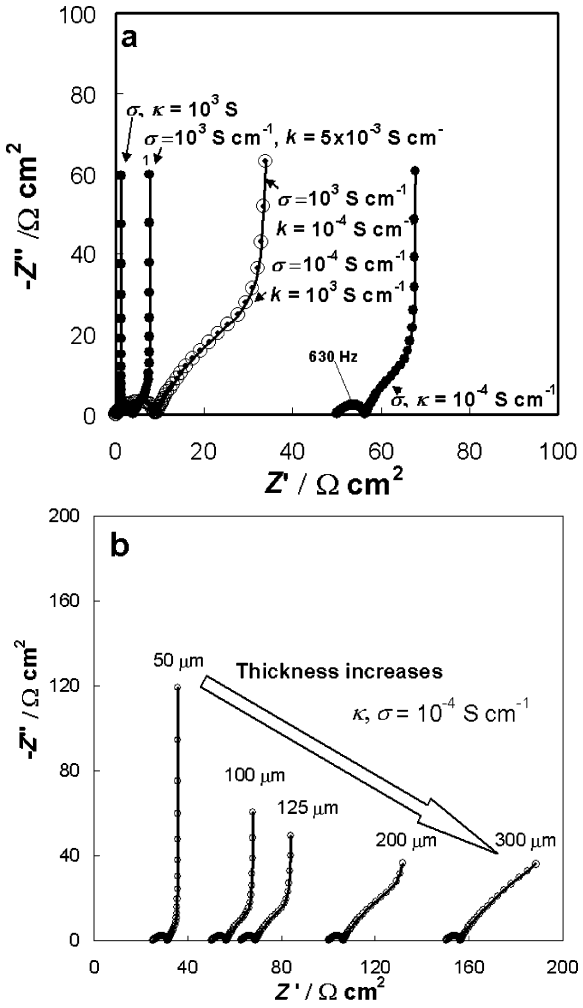

Figure 7. Family of Nyquist plots for a porous electrode composed of a 1:1 mixture of small and large particles with the set of parameters indicated in the caption to Figure 6, except for various combinations of values for κ and σ (a) and thickness of the layer, L, (b) as indicated.

frequency of 0.1 mHz in Figure 5, the true value of the differential intercalation capacitance can be calculated, taking into account the true surface area of the electrode.

Figure 6 shows that a porous electrode composed of particles of different size has basically the same impedance spectra structure as that for porous electrodes comprising particles of a single size, which is in agreement with only a slight dependence of the impedance structure on the particle-size distribution reported by Meyers et al.[19] This signifies that the effect of finite values of σ and κ on the distributed character of the impedance of a porous electrode dominates the effect of the particle-size distribution.

We thus studied the effect of σ and κ on the impedance structure of a porous electrode composed of two particles with radii of 2 and 4 μm ($\theta_1 = 0.5$). Figure 7a shows that the low-frequency arc is formed if at least one of the two conductivities is decreased. Note that eqs 8 and 9 are symmetrical with respect to σ and κ, and thus the same curve was obtained in Figure 7 when σ and κ replace each other (i.e., either the solid particle is highly conductive, whereas the solution is only slightly conductive, or *vice versa*). Next, when both conductivities are low, this causes a drastic shift of the curve along the real impedance axis, as shown in Figure 7a. When both conductivities were fixed at the level of 1×10^{-4} Scm^{-1}, and the thickness of the electrode was increased from 50 to 300 μm, the related Nyquist plots gradually shift to higher Z' values as both the solution resistance in the pores and the bulk electrode resistance increase (see Figure 7b). Within the limit of thin electrodes, the low-frequency capacitance, for example, that "measured" at 0.1 mHz, is proportional to the electrodes' thickness (see Figure 7b). With very thick electrodes this proportionality deteriorates due to the distributed character of the impedance of the porous electrode that influences, and can even dominate, the low-frequency domain.

2.5. Effect of a Passivating Layer Covering the Surface of Inserting Particles. In Figure 1a, the resistance of ion migration through an ion-conducting, but electronically insulating, layer covering the particle's surface is accounted for by a Voigt-type model,[29] according to which a semicircle due to a parallel $R_{sl}||7C_{sl}$ combination is placed in series with the equivalent analogues that simulate the impedance of the inserting particles. The related part of the equivalent circuit analogue is presented at the bottom ofFigure 8. This empiric approach is compared to a slightly different circuit analogue derived theoretically by Meyers et al.[19] (see the top of Figure 8). The difference is that in the latter model, the geometric capacitance of the surface layer is placed parallel to the sum of a Randles-type impedance at the film/particle interface and a surface film resistance, R_{sl}. This is the result of the distribution of the total current between the purely capacitive path (represented by C_{sl}) and the rest of the interfacial impedance, and the active component of the surface-film impedance, that is, precisely in the way as the Randles-type scheme accounts for an interfacial charge transfer and charging of the related double-layer capacitance. If only one of the two charge carriers (an intercalating ion or the counter-balancing electronic species) is assumed to determine the rate of the whole intercalation process, for example, the intercalating ions (and hence, only the interface of the particles with the solution should be considered), the scheme of Meyers et al.[19] seems to be more theoretically substantiated than the Voigt-type scheme.[29] However, it is not at all clear how the other counterbalancing electronic charge carrier affects the impedance behavior. In addition, we were unable to distinguish between the alternative models, as can be seen from the simulated impedance spectra in Figure 8b where the related time constants (i.e., $R_{sl}C_{sl}$ and $R_{ct}C_{ct}$) differ by at least 1 order of magnitude. When these constants were comparable, and hence the two semicircles overlapped, the difference between the models becomes more pronounced, although not so dramatic (see Figure 8c).

As was shown by Zoltowski[38] and Lasia,[39] any three-element RC circuit can be presented by either of the sequences $R_1(R_2||C_2)$ or $(R_1C_2)||R_2$ (similar to the above relation between the Voigt[29] and Meyers et al.[19] models) but with different values of the parameters R_1, R_2, and C_2. If in both cases the different parameters are frequency-independent, this does not mean that both models describe the related electrochemical process adequately. This only implies that in the field of the parameters used it is not possible to distinguish between them. A proper way in solving this problem is to elaborate on the critical parameter, indicating the field of the parameters, within which the alternative models can be distinguished either by frequency dispersion of the parameters, their absolute values, or by the related potential dependences (as was recently demonstrated by us for the alternative in-series combination of finite-length and finite-space Warburgs and two parallel finite-space Warburgs[18]).

Figure 9a compares an overall particle impedance $Z_{part,i}$ (including that due to a surface-layer contribution) calculated

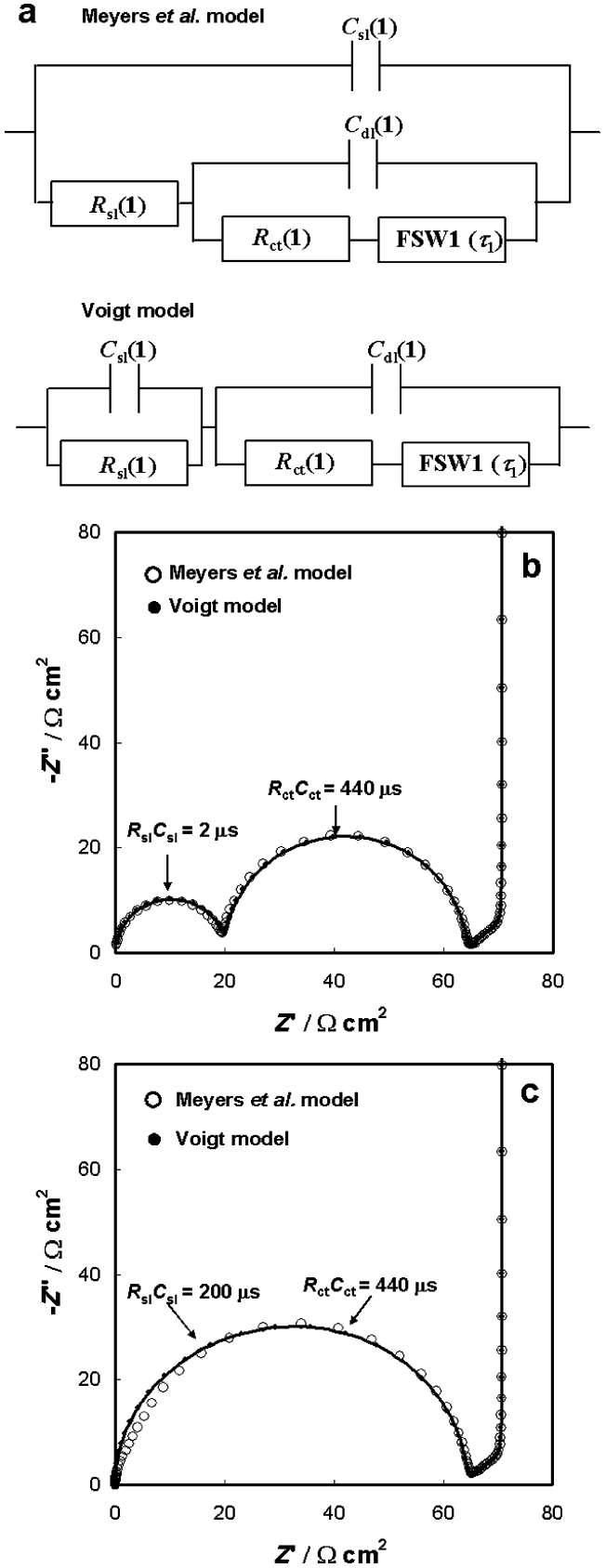

Figure 8. (a) Comparison of the way in which the surface film's capacitance relates to the faradaic branch in the framework of Newman's et al.[19] and Voigt's[29] models; (b) and (c) compares impedance spectra calculated with the use of these models for high and small characteristic time separation between HFS ($R_{sl}||C_{sl}$) and MFS ($R_{ct}||C_{dl}$), respectively. The parameters used were as follows: C_{dif} = 0.317 F, τ_1 = 6.4 s; C_{dl} = 10 μFcm^{-2}; $R_{ct,1}$ = 44.06 Ωcm², $C_{sl,1}$ = 0.1 μFcm^{-2}; $R_{sl,1}$ = 20.0 Ωcm².

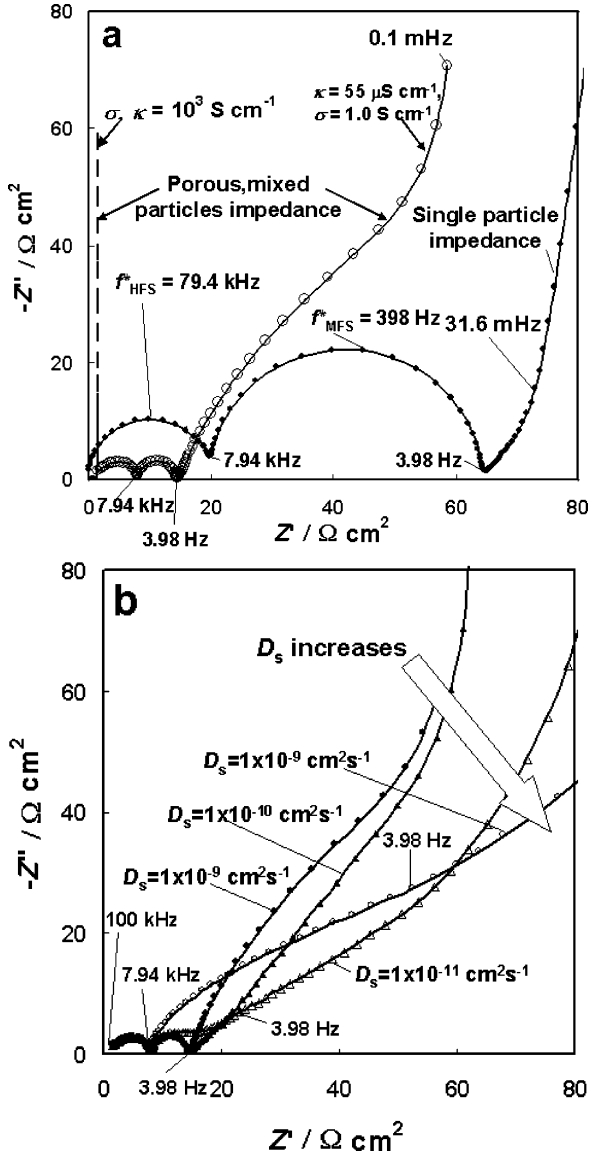

Figure 9. (a) Examples of simulation of impedance spectra for an individual small particle (curve with small dots) and for a porous electrode composed of a 1:1 mixture of small and large particles (marked with larger dots) with the use of a circuit analogue shown in Figure 1a and eqs 5, 8−10. The following parameters of the surface layer were used: $C_{sl} = 1 \times 10^{-7}$ μFcm^{-2} and R_{sl} = 20 Ωcm². Other parameters, including that for the porous structure, were the same as indicated in caption to Figure 6. (b) Simulated Nyquist plots obtained as explained in the caption to Figure 9a with the same parameters, except for the different chemical diffusion coefficient D_s as indicated.

by eq 10, which is analogous, by its form, to that of the impedance for a linear slab particle (eq 4):

$$Z_{part,i} = \frac{R_{ct,i} + \dfrac{R_{part,i}}{Y_{s,i}}}{1 + j\omega\, C_{dl,i}\left[R_{ct,i} + \dfrac{R_{part,i}}{Y_{s,i}}\right]} + \frac{R_{sl,i}}{1 + j\omega\, R_{sl,i}C_{sl,i}} \quad (10)$$

with the impedance for a porous electrode composed of a 1:1 mixture of different size particles (eqs 8, 9, and 10). The time constants were chosen in such a way that the two semicircles were well resolved (separated). Of special interest is the way in which the porous electrode structure affects the high-frequency impedance behavior. When comparing the shape of both the semicircles, one can see that the $R_{sl}||C_{sl}$ semicircle is

flatter at the high-frequency side than the kinetic $R_{ct}||C_{dl}$ semicircle. This is because the distributed character of the impedance for a porous electrode is especially pronounced at high frequencies. In the medium-to-low frequency domain the same arc appears in the impedance spectra in Figure 9a, as was earlier demonstrated in Figures 5 and 6.

Figure 9b shows the effect of changing the value of D_s, on the impedance spectra of a porous electrode. Obviously, because of the good separation between the time constants maintained by the choice of parameters, the $R_{sl}||C_{sl}$ semicircle is not affected, even with pronounced changes in D_s. However, a well-separated $R_{ct}||C_{dl}$ semicircle is formed only when the D_s values become reasonably high; otherwise it strongly overlaps with the low-frequency arc.

2.6. The Effect of a Nonhomogeneous, Multilayered Distribution of a Porous Active Mass of the Electrode. The preparation of composite intercalation electrode coatings, especially manual preparation, may result in a nonhomogeneous distribution of the mass of porous electrodes. To analyze the consequence of such a thickness distribution on the electrode's impedance, we assumed a two-thickness (L_1 and L_2) layer distribution, with a related contribution to the total current of θ_{L1} and $(1 - \theta_{L1})$ (Figure 2). We also assume that each layer is composed of particles of different size with a porous layer impedance that was previously discussed. An extreme combination of thicknesses, 400 and 10 μm, respectively, was chosen here in order to emphasize the nature and origin of the effect of a nonhomogeneous distribution of thicknesses on the electrode impedance. Impedance spectra were first simulated for the two separate porous layers, $Z_{mix,\,L1}$ and $Z_{mix,\,L2}$, (eqs 6, 8, and 9), which were further averaged to determine the total impedance of the parallel combination, Z_{L1+L2}, like the one already considered in Figure 5, according to the expression similar to eq 5:

$$\frac{1}{Z_{L1+L2}} = \frac{\theta_{L1}}{Z_{mix,L1}} + \frac{(1-\theta_{L1})}{Z_{mix,L2}} \qquad (11)$$

We first consider the case of $\theta_{L1} = 0.95$, that is, when a thicker layer, L_1, mainly contributes to the total electrode's capacity.

Figure 10a compares the resulting Nyquist plot for a parallel combination of the two layers, with the related Nyquist plots for the individual layers of thickness, L_1 and L_2. A pronounced low-frequency semicircle with the characteristic frequency of 1.2 mHz appears in the impedance spectrum, in addition to the kinetic, medium-frequency semicircle (a high-frequency semicircle due to surface films can be easily added when relevant, using eq 10). The capacitance (per unit square surface area of the current collector) evaluated from the maximum of Z'' in the semicircle, is large, about 1 F cm^{-2}. A comparison of all three plots helps in understanding the reason for such a high value: the related capacitance has nothing in common with the double layer capacitance and is mainly due to a *secondary* impedance distribution between the two contributing porous layers (primary distribution relates to the porous layers, L_1 and L_2, consisting of particles of different size).

Figure 10a shows that in the limit of very low frequencies, Z_{L1+L2} virtually coincides with the impedance for a thicker layer, L_2 (contributing by a factor of 0.95 to the total capacitance) whereas in the low-to-medium frequency domain (at a characteristic frequency 1.2 mHz) a well-developed semicircle with formally high capacitance of about 1 Fcm^{-2} is formed. The appearance of this semicircle with the above typically high values of capacitance is the most prominent feature of the model of parallel porous sublayers of different thicknesses.

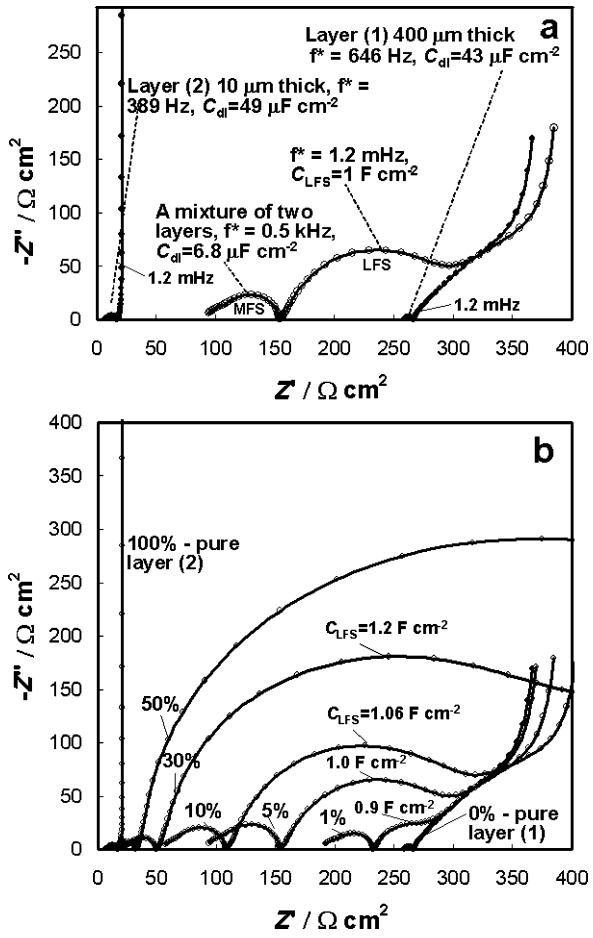

Figure 10. (a) Family of Nyquist plots for a porous electrode composed of a 1:1 mixture of small and large particles (neglecting the effect of surface layers) for inhomogeneous distributed thickness layers. Calculations were performed for $L_1 = 400$ μm (relative fraction 0.95) and $L_2 = 10$ μm (relative fraction 0.05) with the use of eqs 8−11. The characteristic frequencies and the related formal capacitances are indicated. Only the model of geometrical heterogeneity (eq 11) predicts the appearance of well-defined low-frequency semicircle. (b) Simulated impedance spectra similar to that shown in the figure (a) but with a different fraction of thinner layer L_1 from 0 to 100% as indicated.

The above features of the impedance of parallel sublayers can be easily understood from the following qualitative consideration. The impedance of each sublayer in the related frequency range can be *roughly* presented as an in-series combination of the low-frequency resistance and the low-frequency differential (intercalation) capacitance (note that finite values of σ and κ modify the classical finite-space diffusion behavior but this is inessential for the purpose of qualitative consideration). Two limiting cases become immediately clear. In the limit of very low frequency, the impedance of each sublayer is entirely capacitive and since the sublayers are stacked in parallel, the resulting impedance will be mainly affected by the higher differential intercalation capacitance of the thicker layer L_1 compared to that for the thinner layer L_2. In contrast, in the limit of very high frequency, the impedance of each sublayer can be presented by frequency-independent resistances. For the combination of two sublayers under consideration, its reciprocal resistance is simply the weighted sum of the reciprocals of the individual active resistances (compare with eq 11 for the total impedance). This explains the location of the high-frequency limit for the two-sublayer electrode in Figure 10a. However, the most interesting feature appears in the low-to-medium frequency domain. As the frequency increases, the

capacitive contribution to the impedance of the thicker sublayer reduces more strongly than that in the thinner layer because of the higher weight θ_1 and higher intercalation capacitance. Thus, the impedance of the thicker sublayer becomes almost resistive whereas the impedance of the thinner sublayer is still capacitive (see the mutual disposition and frequency dependence of the Nyquist plots in Figure 10a). Since both sublayers are stacked in parallel, the low-frequency capacitance of the thinner sublayer (with a high value compared to that for a typical double-layer capacitance) turns out to be in parallel to the high resistance of the thicker sublayer. We see that in contrast to physically reasonable parallel combinations of the resistance and capacitance such as for the classical Randles scheme ($R_{ct}||C_{dl}$) or for the process of a single-ion migration through a uniform passivation film ($R_{sl}||C_{sl}$), the parallel $R||C$ combination in the proposed model is of a pure geometric reason, namely, because of an uneven coating of the current collector with a porous mass, a problem that the experimentalists may encounter, unless a very careful coating technique is applied.

Figure 10b provides additional information about the dependence of the parameters of thus-formed LFS on the weighting factor of the sublayers distribution. It is seen that as the fraction of the thinnest layer increases up to 0.5, the high-frequency semicircle of the Z_{L1+L2} impedance is very close to that for the thinnest layer. The LFS under discussion has the following characteristic feature: the relevant capacitance calculated from Z''_{max} slightly increases with θ_{L2}, whereas the related resistance also increases. These features can be fully understood in terms of the qualitative description presented above for Figure 10a. Note also that an LFS will be also formed even if all of the intercalation particles have the same radius, but the electrodes are also comprised of thin and thick parts (i.e., two-thickness parameters). However, for the appearance of such an LFS semicircle in the spectra, the values of κ and σ should be low. This effect disappears with the increase in the conductivity values.

It should be noted that low-frequency semicircles have been predicted by a number of models describing, in particular, the diffusion of reacting species in semi-closed pores of different shapes, see Lasia.[39] As was recently shown by Lasia[40,41] the diffusion of the active species in pores results in the appearance of two semicircles on the related Nyquist plots. Particle size distributions discussed, for example, by Diard et al.,[42] may result in a certain inclination toward an arc in the low-frequency. Especially as finite values of σ and κ are taken into account,[19] but never lead to a well-developed semicircle. Barsoukov et al.[43] discussed kinetics of lithium intercalation into carbon anodes within an initial approach to the spherical particles similar to ours, however, their model differed with respect to the description of the porous layer structure in terms of the Paash et al.[44] model. We wish to emphasize once again that the model of parallel stacking of the porous sublayers of different thicknesses described in the present paper refers to a special case of the appearance of LFSs with an extremely high capacitance in their maxima on impedance spectra of porous, composite intercalation electrodes. Further experimental verification of its potentially high significance in comparing the impedance characteristics of single-particle and composite, porous electrodes are in progress in our lab.

3. Conclusion

In this paper, we deal with an analysis of the peculiar low-frequency arcs and well-defined semicircles that reflect very high capacitances that are observed in impedance spectra (presented as Nyquist plots) of a variety of porous, composite cathodes and anodes for rechargeable Li-ion batteries. Whereas the appearance of an arc is explained within the framework of the theory of a porous electrode composed of spherical intercalation particles (Meyers et al.[19]), none of the parameter combinations led to the formation of a semicircle instead of an arc. To reach this conclusion we studied the properties of the Meyers et al[19] model, varying the σ and κ conductivities, the layer thickness, L, the chemical diffusion coefficient D_s, and the porous structure parameter, a, etc. The desired result, that is, the appearance of the low-frequency semicircle with a high capacitance value, could only be achieved by adopting a nonhomogeneous, layered distribution of the active electrode mass. We illustrate this model for an extreme case in which most of the composite electrode comprises a thick layer (400 μm thick, covering 95% of the surface of the current collector), and only 5% of the current collector is covered by a thin layer (10 μm thick). Each sublayer is described within the Meyers et al model.[19] We show that the LFS originates from a parallel combination of a predominantly low-frequency intercalation capacity of the thinner layer and an active, highly resistive component of the impedance of the thicker layer. We also present a detailed comparison between the finite-space diffusion elements for spherical and linear (slab) particles. The relevance of the proposed model to a very common situation in which there are several parallel diffusion paths is discussed (two-parallel diffusion paths in the present case).

References and Notes

(1) Nishizawa, M.; Hashitani, R.; Itoh, T.; Matsue, T.; Uchida, I. *Electrochem. and Solid-State Lett.* **1998**, *1*, 10.
(2) Umeda, M.; Dokko, K.; Fujita, Y.; Mohamedi, M.; Uchida, I.; Selman, J. R. *Electrochim. Acta* **2001**, *47*, 885.
(3) Sato, H.; Takahashi, D.; Nishina, T.; Uchida, I. *J. Power Sources* **1997**, *68*, 540.
(4) Dokko, K.; Mohamedi, M.; Fujita, Y.; Itoh, T.; Nishizawa, M.; Umeda, M.; Uchida, I. *J. Electrochem. Soc*. **2001**, *148*, A422.
(5) Dokko, K.; Mohamedi, M.; Umeda, M.; Uchida, I. *J. Electrochem. Soc*. **2001**, *150*, A425.
(6) Dokko, K.; Nishizawa, M.; Horikoshi, S.; Itoh, T.; Mohamedi, M.; Uchida, I. *Electrochem. and Solid-State Lett.* **2000**, *3*, 125.
(7) Uchida, I.; Mohamedi, M.; Dokko, K.; Nishizawa, M.; Itoh, T.; Umeda, M. *J. Power Sources* **2001**, *97*−*98*, 518.
(8) Shu, D.; Chung, Kyung Yoon; Cho, Won Il; Kim, Kwang-Bum. *J. Power Sources* **2003**, *114*, 253.
(9) Levi, M. D.; Aurbach, D. *J. Phys. Chem. B* **1997**, *101*, 4630.
(10) Levi, M. D.; Aurbach, D. *J. Phys. Chem. B* **1997**, *101*, 4641.
(11) Aurbach D.; Levi, M. D.; Lev, O.; Rabinovich, L.; Gun, J. *J. Appl. Electrochem.* **1998**, *28*, 1051.
(12) Levi, M. D.; Gamolsky, K.; Aurbach, D.; Heider, U.; Oesten, R. *J. Electrochem. Soc.* **2000**, *147*, 25.
(13) Levi, M. D.; Gamolsky, K.; Heider, U.; Oesten, R.; Aurbach, D. *J. Electroanal. Chem.* **1999**, *477*, *32*.
(14) Levi, M. D.; Gamolsky, K.; Heider, U.; Oesten, R.; Aurbach, D. *Electrochim. Acta* **2000**, *45*, 1781.
(15) Levi, M. D.; Salitra, G.; Markovsky, B.; Teller, H.; Aurbach, D. *J. Electrochem. Soc.* **1999**, *146*, 1279.
(16) Aurbach, D.; Levi, M. D.; Levi, E.; Teller, H.; Markovsky, B.; Salitra, G.; Heider, U.; Heider, L. *J. Electrochem. Soc*. **1998**, *145*, 3024.
(17) Levi, M. D.; Aurbach, D. *Electrochim. Acta* **1999**, *45*, 167.
(18) Levi, M. D.; Wang, C.; Aurbach, D. *J. Electroanal. Chem*. **2004**, *561*, 1.
(19) Meyers, J. P.; Doyle, M.; Darling, R. M.; Newman, J. *J. Electrochem. Soc.* **2000**, *147*, 2930.
(20) Pajkossy, T. *J. Electroanal. Chem.* **1994**, *364*, 111.
(21) Franceschetti, D. R.; Macdonald, J. R. *J. Electrochem. Soc*. **1982**, *129*, 1754.
(22) Armstrong, R. D. *J. Electroanal. Chem.* **1986**, *198*, 177.
(23) Gabrielli, C.; Haas, O.; Takenouti, H. *J. Appl. Electrochem*. **1987**, *17*, 82.
(24) Barral, G.; Diard, J.-P.; Montella, C. *Electrochim. Acta* **1984**, *29*, 509.
(25) Montella, C. *J. Electroanal. Chem*. **2002**, *518*, 61.

(26) Franceschetti, D. R.; Macdonald, J. R.; Buck, R. P. *J. Electrochem. Soc*. **1991**, *138*, 1368.
(27) Armstrong, R. D.; Wang, Hong. *Electrochim. Acta* **1994**, *39*, 1.
(28) Mathias, M. F.; Haas, O. *J. Phys. Chem*. **1992**, *96*, 3174.
(29) Macdonald, J. R. *Impedance Spectroscopy*; Wiley: New York, 1987; p.60.
(30) Vorotyntsev, M. A.; Daikhin, L. I.; Levi, M. D. *J. Electroanal. Chem*. **1994**, *364*, 37.
(31) Bisquert, J. *J. Electroanal. Chem*. **2001**, *499*, 112.
(32) Rubinstein, I.; Rishpon, J.; Gottesfeld, S. *J. Electrochem. Soc.* **1986**, *133*, 729.
(33) Levi, M. D.; Markevich, E.; Wang, C.; Koltypin, M.; Aurbach, D. *J. Electrochem. Soc*. (in print).
(34) Armstrong, R. D. *J. Electroanal. Chem*. **1986**, *198*, 12.
(35) Jacobsen, T.; West, K. *Electrochim. Acta* **1995**, *40*.
(36) Ho, C.; Raistrick, I. D.; Huggins, R. A. *J. Electrochem. Soc*. **1980**, *127*, 343.
(37) de Levie, R. Electrochemical response of porous and rough electrodes. In *Advances in Electrochemistry and Electrochemical Engineering*; Delahay, P., Tobias, Ch. W., Eds.; Wiley: New York, 1967; Vol. 6, p 329.
(38) Zoltowski, P. *J. Electroanal. Chem*. **1994**, *375*, 45.
(39) Lasia, A. *Electrochemical Impedance Spectroscopy and Its Applications*, *Modern Aspects of Electrochemistry*; Kluwer Academic/Plenum Publishers: 1999; Vol. 32, p 143.
(40) Lasia, A. *J. Electroanal. Chem*. **1997**, *428*, 155.
(41) Lasia, A. *J. Electroanal. Chem*. **2001**, *500*, 30.
(42) Diard, J.-P.; Le Gorrec, B.; Montella, C. *J. Electroanal Chem*. **2001**, *499*, 67.
(43) Barsoukov, E.; Kim, J. H.; Kim, J. H.; Chul, O. Y.; Lee, H. *Solid State Ionics* **1999**, *116*, 249.
(44) Paash, G.; Micka, K.; Gersdorf, F. *Electrochim. Acta* **1993**, *38*, 2653.